Contribution from the Fachbereich Chemie
der Philipps-Universität, D-3550 Marburg 1, West Germany

Local Bonding Effects and Exchange Interactions in Copper(II) Nitro Complexes $A^I_2B^{II}_{2-x}Cu_x(NO_2)_6$ (A = K, Rb, Tl, Cs; B = Cd, Hg)

A. OZAROWSKI† and D. REINEN*

Received January 7, 1985

Single crystals of the title compounds were investigated mainly by EPR spectroscopy at 9, 35, and 64 GHz and between 4.2 and 300 K. From the hyperfine structure of Cu^{2+} and the nitrogen nuclei in the spectra of the isolated $Cu(NO_2)_6$ moieties, MO coefficients for the in-plane σ bonds, namely $\alpha = 0.87$ and $\alpha' = 0.63$, could be derived. The EPR parameters and their temperature dependence are discussed in terms of the static and dynamic Jahn–Teller effects. In the less dilute complexes exchange-coupled signals due to antiferrodistortive Cu^{2+}–Cu^{2+} pairs with a J value of about 0.6 cm^{-1} additionally appear. Traces of mixed nitro–nitrito-coordinated Cu^{2+} complexes were also detected in the EPR spectra. The presumable geometry of these species could be derived. Finally, superimposed superhyperfine components, induced by the coupling with the Tl nuclei, were observed in the Tl compounds.

Introduction

A wide range of complexes of the general formula $A^I_2B^{II}M^{II}(NO_2)_6$ and with perovskite-related structures is known, in which the A site can be occupied by K^+, Rb^+, Cs^+, or Tl^+ ions and the B and M sites by Ca^{2+}, Sr^{2+}, Ba^{2+}, Pb^{2+}, or Cd^{2+} ions and Ni^{2+}, Co^{2+}, Fe^{2+}, or Cu^{2+} ions, respectively.[1-4] The compounds, which usually have a cubic lattice, may crystallize orthorhombically, if a Jahn–Teller ion (Cu^{2+}, low-spin Co^{2+}) in the six-coordinated octahedral M position with T_h symmetry undergoes partially dynamic or static distortions (Figure 1).[2,6] B is surrounded by twelve oxygen atoms belonging to six NO_2^- ions and also has the site symmetry T_h. A is placed in a site of T_d symmetry, coordinated by twelve oxygen atoms from twelve different NO_2 groups. In particular the copper complexes have been the subject of extensive spectroscopic studies with respect to the Jahn–Teller effect and related phenomena.[1-7] Only one paper dealing with Cu^{2+}-doped nitro complexes has been published so far. EPR g and hyperfine parameters are reported for $Rb_2Pb_{1/3}Cd_{5/3}(NO_2)_6$, $Cs_2PbCd(NO_2)_6$, and $Rb_2Cd_2(NO_2)_6$ with Cu^{2+} in the Cd^{2+} position.[8] Because Zn^{2+}, which is comparable in size to Cu^{2+}, cannot be incorporated into the M position of the described compounds, the much larger Cd^{2+} (and Hg^{2+}) are used as host ions. Because of the large ionic radius of these ions, however, they can also occupy the B sites in nitro complexes. So we used compounds $A^I_2B^{II}_2(NO_2)_6$ (A = Cs, Rb, Tl, K; B = Cd, Hg), which are partly described in the literature already,[9] as host lattices. In the following we report the results of mainly EPR investigations on mixed crystals $A_2B_{2-x}Cu_x(NO_2)_6$. Since it was possible to obtain single crystals over a broad range of x, one could observe phenomena due to isolated copper polyhedra in the diluted samples and on the other hand various cooperative effects, such as exchange interactions, in the semidiluted and concentrated samples. The compounds are also characterized by X-ray analysis and electronic spectroscopy in the ligand field region (powder investigations).

Experimental Section

Synthesis. The complexes $A^I_2B^{II}_{2-x}Cu_x(NO_2)_6$ [A^I = K, Rb, Tl, Cs; B^{II} = Cd, Hg] were prepared in a similar way as previously described.[2] A solution of u mol of $B(NO_3)_2$ and w mol of $Cu(NO_3)_2 \cdot 5H_2O$ ($u + w = 0.02$) in about 5 mL of H_2O was added with stirring to a solution of 0.06 mol of $NaNO_2$ and 0.02 mol of ANO_3 in 5–10 mL of H_2O at 50–70 °C. The powder products precipitated from the solution upon cooling. Single crystals could be obtained from the mother liquor by slow cooling (0.2 °C/h). The Cu/B ratio in the solid was always smaller than the one in solution. This difference was considerable at high and not significant at low Cu^{2+} concentrations. The achievable range of the Cu^{2+} concentration in single crystals was $x = 10^{-4}$–0.86 for $K_2Cd_{2-x}Cu_x(NO_2)_6$ and $x = 10^{-3}$–0.2 for compounds with Rb, Tl, or Cs. In the powder samples with Cd a doping level up to $x = 1$ was possible. However, these concentrated samples contained too much A with respect to Cd and Cu. The stoichiometry was correct up to $x \simeq 0.9$, 0.7, and 0.3 for the compounds with K, Tl, and Cs, respectively. During our attempts to prepare the concentrated samples, we obtained new compounds $A_4A'Cu_3(NO_2)_{11}$ (A, A' = Cs, K; Cs, Na; Rb, K; Rb, Na), which crystallize in a cubic structure.[10] The analyses were carried out by atomic absorption. Some dilute samples were prepared with ^{63}Cu, in order to analyze the EPR hyperfine and superhyperfine structure. The available ^{63}CuO (Oak Ridge National Laboratory) was dissolved in nitric acid.

Structural Measurements. X-ray powder diagrams were recorded on a Philipps 1049/10 instrument with a PW 1050/25 goniometer (Cu Kα radiation). Si was used for calibration purposes.

Electronic Spectra. The electronic reflectance spectra at 298 K were measured with a Zeiss DMR-21 instrument for powder samples, with Sr_2ZnTeO_6 and MgO used as standards in the 4000–12000- and 8000–40000-cm^{-1} ranges, respectively.

EPR Spectra. The EPR spectra were recorded on a Varian E15 spectrometer at 9 and 35 GHz, in the temperature range 4.2–300 K. We could also observe the spectra of more concentrated samples at 60 ± 4 GHz, though the sensitivity was comparatively low. In one case even the ^{14}N superhyperfine structure could be detected ($Cs_2Hg_{1.9}Cu_{0.1}(NO_2)_6$, 77 K) at this frequency. The sample was placed directly in a section of the shortened waveguide, and no cavity was employed. An OKI 60 V 10 klystron and Baytron 2 V-1 isolator, 3 V-1 attenuator, 3 V-88 magic T, and 3 V-90 tuner were used. The signal from the V-band microwave diode was supplied to the preamplifier input of the Q-band microwave unit and was processed further in the usual way.

Table I. Unit Cell Dimensions of $A_2BB'(NO_2)_6$ Complexes

A	B	B'	a, Å	c, Å	δ[a]
K	Cd	Cd	7.59_0	18.25	-1.8_5
Rb	Cd	Cd	7.62_4	18.45_5	-1.1_5
Tl	Cd	Cd	7.62_0	18.45	-1.1_5
Cs	Cd	Cd	7.72_5	18.81	−0.6
Tl	Hg	Hg	7.73_0	18.67_5	-1.3_5
Cs	Hg	Hg	7.83_3	19.07_5	−0.6
Cs	Pb	Hg	11.26_8		0

[a] Deviation from cubic symmetry: $100(c/a - 6^{1/2})/6^{1/2}$%.

Results

Structural Data. The X-ray powder patterns of the host compounds (and also of the diluted Cu^{2+} complexes) could be indexed on the basis of a hexagonal unit cell (Table I). The structure closely resembles the ordered perovskite lattice, but with a small compression along a 3-fold axis. The more concentrated copper compounds are cubic. The hexagonal ↔ cubic phase transitions for the Cd complexes occur at $x \simeq 0.1$ (Cs) and $x \simeq 0.2$ (Rb, Tl, K). From the unit cell dimensions of the cubic mixed crystals,

†On leave from Institute of Chemistry, Wroclaw University, Wroclaw, Poland.

(1) Elliott, H.; Hathaway, B. J.; Slade, C. R. *Inorg. Chem.* **1966**, *5*, 669.
(2) Reinen, D.; Friebel, C.; Reetz, K. P. *J. Solid State Chem.* **1972**, *4*, 103.
(3) Barnes, J. C.; Duncan, C. S.; Peacock, R. D. *J. Chem. Soc., Dalton Trans.* **1972**, 1875.
(4) Hitchman, M. A.; Rowbottom, G. L. *Coord. Chem. Rev.* **1982**, *42*, 55.
(5) Hathaway, B. J.; Billing, D. E. *Coord. Chem. Rev.* **1970**, *5*, 143.
(6) Reinen, D.; Friebel, C. *Struct. Bonding (Berlin)* **1979**, *37*, 1.
(7) Hathaway, B. J. *Coord. Chem. Rev.* **1982**, *41*, 423.
(8) Joesten, M. D.; Venable, J. H. *Inorg. Chem.* **1983**, *22*, 1733.
(9) Ferrari, A.; Cavalca, L.; Nardelli, M. *Gazz. Chim. Ital.* **1935**, *65*, 797.
(10) Ozarowski, A.; Allmann, R.; Reinen, D., submitted for publication.

0020-1669/85/1324-3860$01.50/0

Table II. Single-Crystal EPR Data of Compounds $A_2B_{2-x}Cu_x(NO_2)_6$

	T, K	g_x	g_y	g_z	$\lvert A_z\rvert$, 10^{-4} cm^{-1}	μ	ϕ, deg
A = K, B = Cd	298	2.050	2.098	2.265	145	0.035	−12.3
x = 0.002	77	2.049	2.083	2.270	163	0.035	−8.2
	4.2	2.053	2.070	2.268	169	0.034	−4.1
A = Rb, B = Cd	298	2.052	2.100	2.268	145	0.036	−12.2
x = 0.01	77	2.053	2.083	2.274	157	0.035	−7.2
	4.2	2.056	2.072	2.268	162	0.034	−3.9
A = Cs, B = Cd	77	2.053	2.078	2.280	160	0.035	−5.8
x = 0.06	4.2	2.059	2.073	2.275	166	0.035	−3.3
A = Tl, B = Cd	298	2.051	2.098	2.261	144	0.034	−12.3
x = 0.03	77	2.051	2.084	2.271	153	0.035	−8.0
A = Cs, B = Hg	77	2.052	2.070	2.255	166	0.032	−4.6
x = 0.1	4.2	2.055	2.070	2.257	174	0.033	−3.8

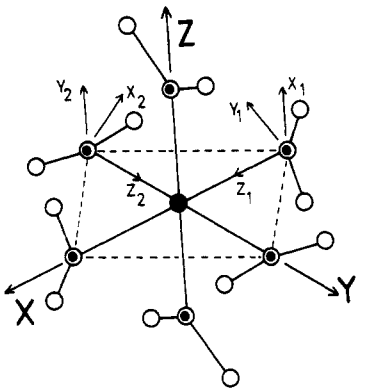

Figure 1. Structure of a molecular $Cu(NO_2)_6^{4-}$ complex with D_{2h} symmetry [typical Cu–N bond lengths: 2.03–2.04 Å (x), 2.04–2.05 Å (y), and 2.31 Å (z)]. The coordinate systems for two types of nitrogen atoms are also shown.

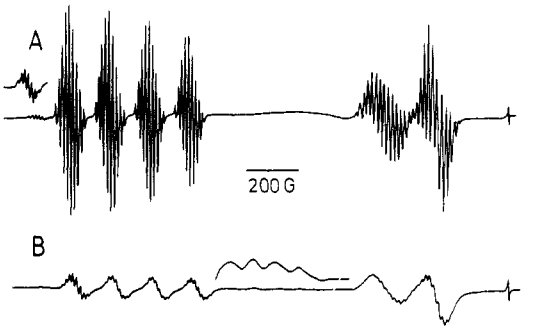

Figure 2. (A) Single-crystal Q-band (77 K) spectrum of $K_2Cd_{1.998}Cu_{0.002}(NO_2)_6$ parallel to a crystal axis (θ = 0°). The additional signal on the low-field side was recorded at θ = 10°. (B) Single-crystal Q-band spectrum (77 K) of $K_2Cd_{1.98}Cu_{0.02}(NO_2)_6$, showing also the signals due to exchange-coupled pairs.

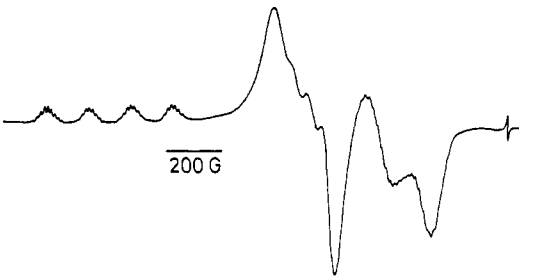

Figure 3. Powder Q-band (77 K) spectrum of $K_2Cd_{1.998}Cu_{0.002}(NO_2)_6$.

which decrease linearly with the copper concentration, the lattice constants for the hypothetical compounds $K_2CdCu(NO_2)_6$ and $Tl_2CdCu(NO_2)_6$ could be extrapolated. They are 10.46 and 10.53 Å, respectively, and are consistent with the data of other nitro complexes.[2,6]

Ligand Field Spectra. The reflectance spectra show only two broad and badly resolved absorptions around 8500 and 15 500 cm^{-1}. The two bands can be assigned to the transitions $^2_aA_{1g}(x^2 - y^2) \rightarrow {}^2_bA_{1g}(z^2)$ and $^2_aA_{1g} \rightarrow {}^2B_{1g}$, $^2B_{2g}$, $^2B_{3g}$ in D_{2h} symmetry, which results from the T_h symmetry of the $Cu(NO_2)_6$ polyhedra, if one includes a static Jahn–Teller distortion and neglects the tiny hexagonal unit cell deformation.

EPR Spectra—General Data. The main features of the EPR spectra between 298 and 4.2 K are orthorhombic signals with closely lying, but still well-separated, g_x and g_y values at Q- and V-band frequencies. The hyper- and superhyperfine structures are well resolved at low x values (Figure 2). The spin-Hamiltonian parameters obtained from the powder and single-crystal spectra are identical. The A_z(Cu) and g values—in particular g_y—were temperature-dependent, however (Table II).

Additionally the spectra exhibit a signal around $g \simeq 2.13$ with a nicely resolved hyperfine structure corresponding to $A = 70 \times 10^{-4}$ cm^{-1} (Figure 3). The HF structure is observed only for very diluted samples ($x \leq 0.002$), however. The signal does not change position with the orientation of the crystal. The intensity decreases when the temperature is lowered, and the signal vanishes at 4.2 K. The isotropic g value is exactly the arithmetic average of the orthorhombic g_x, g_y, and g_z components. The A value also equals—within the experimental error—$(A_x + A_y + A_z)/3$. This part of the spectra is obviously due to the dynamic Jahn–Teller effect[11,12] and results from a fast reorientation of the long axis in the elongated octahedra of CuN_6 with respect to the EPR time scale. The isotropic signal is weak in the spectra of single crystals, whereas it is a dominant feature of the powder spectra (Figure 3). Such a behavior has been observed previously[13,14] and has been attributed to structural changes during the preparation of powdered samples. However, in our opinion the reason is different. The single-crystal spectrum reflects the intensity ratio R between the isotropic and anisotropic spectra correctly. In the powder spectrum the intensity of the anisotropic absorption is distributed over the entire field range between $g_\parallel$ and $g_\perp$, while the isotropic part remains as intensive as in the single-crystal spectrum. It can be shown that the apparent enhancement of the intensity ratio R in the powder spectrum with respect to the R value in the single-crystal spectra is of the order of magnitude $(H_\perp - H_\parallel)/3\Gamma$, where Γ is the line width. The enhancement can be easily as large as 100 at Q-band frequency.

In the spectra of more concentrated samples ($x > 0.1$) a second isotropic signal appears.[6] The position of the signal is concentration-dependent and varies between $g = 2.13$ for the lower and $g = 2.12$ for the highest x values. It does not show hyperfine splittings and remains at 4.2 K. The orthorhombic spectrum is still visible with unchanged parameters. In our opinion this line

(11) Abragam, A.; Bleaney, B. "Electron Paramagnetic Resonance of Transition Ions"; Clarendon Press: Oxford, England, 1970.
(12) Sturge, D. M. *Solid State Phys.* **1968**, *20*, 91.
(13) Friebel, C. *Z. Anorg. Allg. Chem.* **1975**, *417*, 197.
(14) Ammeter, J. H.; Bürgi, H. B.; Gamp, E.; Meyer-Sandrin, V.; Jensen, W. P. *Inorg. Chem.* **1979**, *18*, 733.

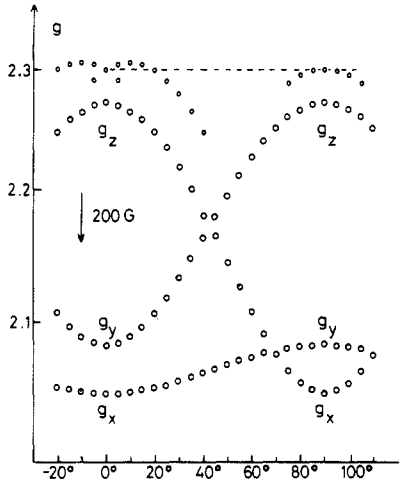

Figure 4. Angular dependencies of the resonance fields for $K_2Cd_{1.998}Cu_{0.002}(NO_2)_6$ at 77 K. The top part refers to the weak low-field spectrum (see text).

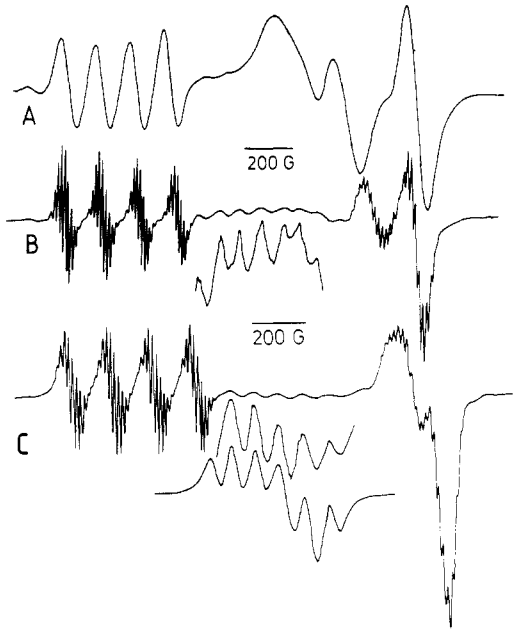

Figure 5. Single-crystal Q-band EPR spectra of $Rb_2Cd_{1.98}Cu_{0.02}(NO_2)_6$ parallel to a crystal axis ($\theta = 0°$) at 298 K (A), 77 K (B), and 4.2 K (C), showing also signals due to exchange-coupled, antiferrodistortive pairs. The lowest curve in spectrum C is calculated ($J = 0.6$ cm^{-1}, $X = 14 \times 10^{-4}$ cm^{-1}, $Y = 16 \times 10^{-4}$ cm^{-1}, $Z = -32 \times 10^{-4}$ cm^{-1}, $g_x = 2.05$, $g_y = 2.07$, $g_z = 2.27$, $A_x = 20 \times 10^{-4}$ cm^{-1}, $A_y = 30 \times 10^{-4}$ cm^{-1}, $A_z = 160 \times 10^{-4}$ cm^{-1}).

is a result of exchange interactions between three $Cu(NO_2)_6$ moieties, which are oriented orthogonally with respect to each other. Since the signal does not split even at 64 GHz, the energy of the exchange interactions must be comparable to or larger than the V-band quantum energy ($J \gtrsim 2$ cm^{-1}). In the spectra of very concentrated samples ($x > 0.4$) only the latter type of signal could be observed. The orthorhombic spectrum and the dynamic signal, characteristic for isolated $Cu(NO_2)_6$ polyhedra, disappear completely.

In some cases signals due to exchange-coupled pairs are observed ($0.001 \leq x \leq 0.1$), which appear at $g = (g_\parallel + g_\perp)/2$ and exhibit a hyperfine structure corresponding to $A = 90 \times 10^{-4}$ cm^{-1} (Figures 2B and 5B,C).

On the low-field side of the spectra with small Cu^{2+} concentrations ($x < 0.1$) a weak signal with an intensity of about 1/40 with respect to that of the main spectrum is observed both for powders and single crystals (Figure 2).

The angular dependencies of the **g** and hyperfine tensors were obtained by using big single crystals of tetragonal shape ($2 \times 2 \times 1$ mm^3) (Table II, Figure 4). They were identical in the three orthogonal planes. We observed three signals of equal intensities due to the presence of three CuN_6 moieties with mutually perpendicular orientation in each plane. The main axes of the **g** tensor were parallel to the crystal axes. The z directions of the **g** and **A**(Cu) tensors coincided. The orientations of the x and y axes of the **g** tensor with respect to those of the corresponding hyperfine tensor components could not be determined; these axes were assumed to be parallel also. At low temperatures the superhyperfine structure due to two slightly inequivalent ^{14}N pairs in the xy plane was resolved.

Table III. Hyperfine Coupling Constants (10^{-4} cm^{-1}) of $K_2Cd_{1.998}Cu_{0.002}(NO_2)_6$, Derived from the 77 K Q-Band Spectrum[a]

	Cu	N_1	N_2
$\|A_x\|$	17.2	13.0 (12.5)	12.6 (12.8)
$\|A_y\|$	31.1	13.0 (13.2)	14.3 (13.8)
$\|A_z\|$	163.0	16.0 (16.2)	16.6 (16.8)

[a] The values corrected for superhyperfine dipole–dipole interactions are given in parentheses.

The analysis of the weak, low-field part of the spectrum (Figure 2) showed that this signal was a Cu^{2+} hyperfine component with a peculiar angular dependence (Figure 4). The—temperature-independent—g_z and A_z values for this spectrum were 2.305 and 150×10^{-4} cm^{-1}, respectively. The "perpendicular" parameters could be not derived directly, because the intense spectrum and the weak one overlapped. Fortunately, the weak signal could be observed over a range of ±30° from the extreme position (Figure 4), and this allowed us to estimate the g_{xy} value ($\simeq 2.06$). The signal showed a superhyperfine structure consisting of seven lines and hence gives evidence of an interaction with only three nitrogen nuclei in the xy plane. It could be deduced from the angular dependence of this pattern that four molecular units are present, for which the z axes are tilted with respect to the z axis of the regular molecule by ±10° and ±170° in the xz plane.

EPR Spectra—Hyperfine and Superhyperfine Structure. In the g_z part of the nicely resolved spectra of the diluted compounds ($10^{-4} < x < 10^{-1}$), a nine-line SHF structure was detected. As computer simulations demonstrated, this structure is due to two pairs of nitrogen atoms with coupling constants of 13.0×10^{-4} and 14.3×10^{-4} cm^{-1}, respectively. The analysis of the g_x and g_y part was intricate because the Cu^{2+} hyperfine constant was comparable to the nitrogen SHF constants. Only the spectra of $K_2Cd_{1.998}Cu_{0.002}(NO_2)_6$ and $Rb_2Cd_{1.98}Cu_{0.02}(NO_2)_6$ recorded at 77 K had a sufficient quality for the simulation. At the high magnetic field required for the Q-band measurements the hyperfine and superhyperfine splittings for arbitrary orientations can be described in very good approximation by the effective Hamiltonian

$$\hat{H} = \mathbf{g}\beta\mathbf{H}\hat{S}_z + \mathbf{A}(\mathrm{Cu})\,\hat{S}_z\,\hat{I}_z(\mathrm{Cu}) + \sum_{\mathrm{lig}}\mathbf{A}(\mathrm{L})\,\hat{S}_z\,\hat{I}_z(\mathrm{L}) \quad (1)$$

where "**g**" and "**A**" are the projections of the corresponding tensors on the magnetic field direction. Nuclear quadrupole interactions were neglected. If we refer to the coordinate systems of the nitrogen atoms in the xy plane (Figure 1) the hyperfine structures in g_z are determined by $A_z(\mathrm{Cu})$, $2A_x(N_1)$, and $2A_y(N_2)$, those in g_y by $A_y(\mathrm{Cu})$, $2A_z(N_1)$, and $2A_x(N_2)$, and finally those in g_x by $A_x(\mathrm{Cu})$, $2A_z(N_2)$, and $2A_y(N_1)$. The axial nitrogen atoms were assumed to be inactive as far as the SHF splitting is concerned.[15] This is indeed expected for the ground state of Cu^{2+}, which is predominantly $d_{x^2-y^2}$. A splitting of only 0.7 G due to the axially coordinated pyridine ligand has been observed for Cu(acac)py by ^{14}N NMR contact shift measurements.[15] In our case, as has been proven by the simulation of the g_z part of the spectra, the splitting must be smaller than 0.5 G. The simulation procedures yielded the set of parameters in Table III. The errors of the coupling constants are not easy to estimate, but a change of 0.5

(15) Wayland, B. B.; Wisniewski, M. D. *J. Chem. Soc. D* **1971**, 1025.
(16) Pople, J. A.; Schneider, W. G.; Bernstein, H. J. "High Resolution NMR"; McGraw-Hill: New York, Toronto, London, 1959; p 485.
(17) Clack, D. W.; Reinen, D. *Solid State Commun.* **1980**, *34*, 395.

$\times 10^{-4}$ cm^{-1} produced already significant changes in the spectra. We may hence assume that the errors are smaller than 1×10^{-4} cm^{-1}. The superhyperfine constants have to be corrected for the dipole–dipole interaction, in order to obtain the contact term, which is usually considered to reflect the covalency of the Cu–N bonds. The dipolar contribution to the SHF interaction is

$$A_d(2\hat{I}_z\hat{S}_z - \hat{I}_x\hat{S}_x - \hat{I}_y\hat{S}_y) \quad (2)$$

with $A_d = (g_e\beta_e g_N\beta_N)/r^3$ [11,16] (g_N and β_N refer to the ^{14}N nucleus). For a Cu–N spacing of $r = 2.05$ Å one obtains $A_d = 0.25 \times 10^{-4}$ cm^{-1}. Thus, $-2A_d$ and $+A_d$ have to be added to the SHF constants measured at $H \parallel z$ and $H \perp z$, respectively (Table III). The two pairs of nitrogen atoms, N_1 and N_2, are almost identical if SHF constants of positive sign are assumed, and are also in accord with an axial symmetry of the ^{14}N SHF tensor; the differences between the respective A_x and A_y values are well within the experimental error range. Hence we will use the following averaged parameters in our calculations: $A_\perp = 13.1 \times 10^{-4}$ cm^{-1}; $A_\parallel = 16.5 \times 10^{-4}$ cm^{-1}; $A_{iso} = 14.2 \times 10^{-4}$ cm^{-1}.

Discussion

EPR Spectra of Isolated $Cu(NO_2)_6$ Polyhedra. The pronounced nonaxiality of the **g** and **A**(Cu) tensors is an obvious result of the admixture of the d_{z^2} orbital to the $d_{x^2-y^2}$ ground state. The magnitude of this admixture is dependent on the actual symmetry of the CuN_6 moieties distorted by the Jahn–Teller effect and can be expressed in terms of the angular parameter ϕ, which defines the minima in the lower surface of the "Mexican hat" potential ($E \otimes \epsilon$ vibronic coupling). The ground-state wave function[11,18]

$$\Psi = [\sin(\phi/2)]d_{z^2} + [\cos(\phi/2)]d_{x^2-y^2} \quad (3)$$

and the g values are strongly dependent on ϕ:

$$g_x = g_0 + 4u_x - 2(u_y^2 + u_z^2) - (u_xu_y - u_yu_z + u_zu_x) - [2u_x + 2(u_z^2 - u_y^2) - (2u_xu_y + u_yu_z - u_zu_x)]\cos\phi + 3^{1/2}[2u_x + u_y^2 - (u_yu_z + u_zu_x)]\sin\phi \quad (4)$$

$u_i = k_i^2\lambda_0/E_i$ ($i = x, y, z$) are the orbital contributions, k_i the covalency parameters, and the E_i the ligand field transitions to the d_{yz}, d_{xz}, and d_{xy} orbitals. g_y and g_z can be generated from the above formula by cyclic permutation of u_x, u_y, and u_z and by changing ϕ by $4\pi/3$ every time.[6] Because the ortho-rhombicity of the EPR spectrum is quite small, it is reasonable to assume $u_x = u_y = u_\perp$ ($u_z = u_\parallel$). We have calculated the u and ϕ values for several complexes and at different temperatures (Table II). Because we have found that $u_\parallel$ and $u_\perp$ are equal within the error limit, only one u value is listed. The presumable reason for the isotropy of u is the weak π-bonding activity of the nitro ligands (see below).[17] The orthorhombic spectrum is due to CuN_6 polyhedra, which are statically Jahn–Teller distorted. A lower symmetry than tetragonal is expected, because the vibronic coupling of the E_g ground state with the ϵ_g vibrational mode does not transform the T_h geometry of the $Cu(NO_2)_6$ octahedra in cubic nitrocomplexes (Figure 1) into D_{4h} but into the lower D_{2h} site symmetry. The small trigonal lattice distortion—if present—should also induce geometries lower than tetragonal. The presence of the orthorhombic spectrum already at 298 K indicates lattice strains of appreciable magnitude, which significantly lower one of the three minima in the ground-state potential surface with respect to the other two. This strain is presumably due to the great difference between the sizes of the Cd^{2+} and Cu^{2+} ions, which occupy the same M^{II} site and hence support local anisotropies in the mixed crystals. The temperature dependence of the **g** and **A** tensors—in particular of g_y—is obviously correlated with an increase of the orthorhombic distortion component, which is described by the angular parameter ϕ, with increasing temperature (Table II). We think that a population of excited vibronic levels in the potential curve of the lowest of the three minima and an averaging by fast relaxation cause this effect.[19] The isotropic signal characterizes the dynamic averaging over the three potential minima, due to the excitation of even higher vibronic states. The intensity ratio between the isotropic and orthorhombic spectra, which decreases toward zero going to 4.2 K (Figure 5), also depends on the constitution of the compounds. It increases appreciably, if one substitutes K by Rb or Tl and further, if Cs occupies the A position (Figures 5B and 6C). Obviously the strain becomes weaker and hence the energy difference between the lower minimum and the other two wells smaller, if the size of the A cation increases and the trigonal lattice distortion diminishes.

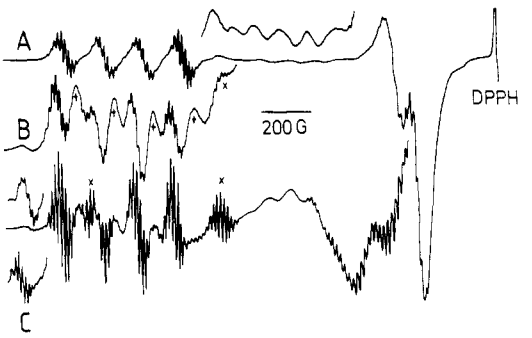

Figure 6. Single-crystal EPR Q-band spectra of $Cs_2Cd_{2-x}Cu_x(NO_2)_6$ parallel to a crystal axis ($\theta = 0°$), for $x = 0.08$ at 4.2 K (A) and 77 K (B) and for $x = 0.06$ at 77 K (C). Besides the main spectrum (I) two further spectra of probably the same symmetry are visible (× = II; + = III). Signals due to the nitro–nitrito species are also shown [$\theta = 0°$ and $\theta = 10°$ (below)].

The X-band powder spectrum reported for Cu^{2+}-doped $Rb_2Cd_2(NO_2)_6$[8] shows weak absorptions near the third and fourth hyperfine components of the $g_\parallel$ signal, which are ascribed to Cu^{2+} in the 12-coordinated B position and to dynamic CuN_6 moieties, respectively. These peaks are the second and third A components of the hyperfine quartet of the isotropic signal, however, which clearly follows from our much better resolved Q-band spectra and their temperature dependence.

The A_z hyperfine constant of the orthorhombic spectrum could be observed directly, because the g_z signal is always nicely split (Figures 2 and 5). A_x and A_y were found by the simulation of the 77 K Q-band spectrum of $K_2Cd_{1.998}Cu_{0.002}(NO_2)_6$, which is particularly well resolved (Table III). The 4.2 K values of A_x and A_y are presumably slightly lower, in analogy to A_z, which increases if the temperature is lowered.

The spectra of the Cs–Cd compounds are—in contrast to those of all the other complexes—more complicated (Figure 6). The interesting feature is the presence of at least three different orthorhombic spectra, I, II, and III, besides the isotropic signal. They seem to be correlated with the same vibronic ground state, however, because only one orthorhombic spectrum remains at 4.2 K. We could exclude that the additional spectra II and III are induced by exchange coupling, mainly because they are not observed at X-band frequency. Obviously they are visible in the Q-band because of their different g values rather than because of zero-splitting effects or a change of the Q-ratio (see the section on exchange interactions). The g values listed in Table II refer to the main spectrum I. The origin of spectra II and III is doubtful. The g_z values of II, in which the hyperfine structure is as well resolved as in I, and III are about 2.25_5 and 2.26_5, respectively. Spectra II and III are possibly due to excited vibronic states in the lowest potential well. This explanation presumes that the relaxation between the ground and excited states is not fast enough, especially for these compounds, however.[19] An alternative explanation for the dynamic spectrum III, which does not show nitrogen hyperfine structure, is a small fraction of Cu^{2+} in the

(18) Bleaney, B.; Bowers, K. D.; Pryce, M. H. L. *Proc. R. Soc. London, A* **1951**, *230*, 166.
(19) Riley, M. J.; Hitchman, M. A.; Reinen, D., submitted for publication.
(20) Kivelson, D.; Neiman, R. *J. Chem. Phys.* **1961**, *35*, 149.
(21) Guzy, C. M.; Raynor, J. B.; Symons, M. C. R. *J. Chem. Soc. A* **1969**, 2299.
(22) Hartree, D. R.; Hartree, W. *Proc. R. Soc. London, A* **1948**, *100*, 299.
(23) Abragam, A.; Pryce, M. H. C.; Horowitz, J. *Proc. R. Soc. London, A* **1955**, *230*, 169.

oxygen-coordinated B site (cf. ref 8). It may not be detected any more because of intensity reasons, if it is frozen in at 4.2 K. The investigations, in particular with respect to the Cs–Cd mixed crystals, will be continued.

Bonding Parameters of $Cu(NO_2)_6$ Moieties. The molecular orbital expression for the unpaired electron of Cu^{2+} in the considered compounds is

$$\Phi = \alpha\psi - \alpha'\psi_L \tag{5}$$

where ψ is the ionic ground-state function in eq 3 and ψ_L is the symmetry-adapted combination of ligand s and p orbitals. α can be calculated from the hyperfine parameters A(Cu). We have modified the formulas of Ammeter[24] such that we could use the experimental g values instead of the orbital contributions u_i:

$$A_z = P\left[(-\kappa - {}^4/_7\cos\phi)\alpha^2 + \frac{g_x - g_0}{14}\frac{3 - 2(3^{1/2})\sin\phi}{2\cos\phi - 1} + \frac{g_y - g_0}{14}\frac{3 + 2(3^{1/2})\sin\phi}{2\cos\phi - 1} + g_z - g_0\right] \tag{6}$$

With the g, A_z, and ϕ values taken from the EPR spectrum of $K_2Cd_{1.998}Cu_{0.002}(NO_2)_6$ at 4.2 K (Table II) and a negative sign for A_z(Cu), we obtained $\alpha = 0.87$, if $P = 0.036$ cm^{-1} and $\kappa = 0.43$[11,18,20-23] are used in the calculation. A_z was very sensitive to small variations of α but only weakly sensitive with respect to small changes of ϕ. The A_x and A_y components, as calculated with $\alpha = 0.87$, are -16.2×10^{-4} and -29.7×10^{-4} cm^{-1}, in reasonable agreement with the experimental data (Table III).

The MO coefficient α' is accessible from the nitrogen SHF structure in the EPR spectrum. The isotropic part of the coupling constants is due to the s-electron density at the ^{14}N nucleus[11]

$$A_{iso} = \frac{8\pi}{3}g_e\beta_e g_N\beta_N|\psi_{2s}|^2c_s^2 = A^s_N c_s^2 \tag{7}$$

while the p-electron density contributes only to the anisotropic part of the SHF structure

$$A_\parallel = A_{iso} + {}^4/_5A_{ani} \qquad A_\perp = A_{iso} - {}^2/_5A_{ani}$$
$$A_{ani} = g_e\beta_e g_N\beta_N\langle r_{2p}^{-3}\rangle c_p^2 = A^p_N c_p^2 \tag{8}$$

c_s and c_p are the MO coefficients of the 2s and 2p orbitals of nitrogen and are directly related to α' in eq 5. A^s_N and A^p_N are calculated to be 0.0532 cm^{-1} and 40.1×10^{-4} cm^{-1}, respectively, if the values reported in[22] were taken for $\langle r_{2p}^{-3}\rangle$ and $|\psi_{2s}|^2$. We derived $c_s = 0.164$ and $c_p = 0.268$ from the experimental $A_\parallel$ and $A_\perp$ values by applying eq 7 and 8. The density of the unpaired electron of Cu^{2+} at one nitrogen nucleus is then $c_s^2 + c_p^2 = 0.0987$ and must be also equal to $\alpha'^2/_4$ ($\alpha' = 0.63$). Because the angular parameter ϕ deviates only little from the tetragonal value of 0° and hence the d_{z^2} contribution to φ (eq 3) can be neglected in good approximation, the ligand function is

$$\psi_L = {}^1/_2(-\sigma_1 + \sigma_2 + \sigma_3 - \sigma_4) \qquad \sigma_i = np_i + (1 - n^2)^{1/2}s_i \tag{9}$$

and we may now write down the complete ground-state function

$$\Phi = 0.87(d_{x^2-y^2}) - 0.63[0.85({}^1/_2(-p_1 + p_2 + p_3 - p_4)) + 0.52({}^1/_2(-s_1 + s_2 + s_3 - s_4))] \tag{10}$$

The normalization condition for Φ leads to 0.140 for the sum of the group overlap integrals between $d_{x^2-y^2}$ and the ligand s and p LCAO's. If the standard overlap integrals of Smith[25] are used, 0.18 results for this sum. The agreement is reasonable, if one considers the rather complicated procedure for obtaining the MO coefficients. The ratio R of the ligand p and s coefficients is 1.6 and is approximately in accord with an sp^2 hybridization ($R = 1.4$).

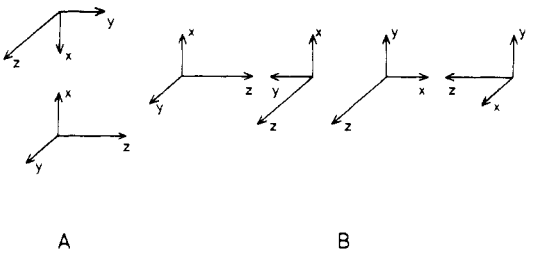

A B

Figure 7. Antiferrodistortive patterns in Cu^{2+} nitro complexes: intrachain (A) and interchain interactions (B) in $K_2PbCu(NO_2)_6$ and possible pair geometries in compounds $A_2Cs_{2-x}Cu_x(NO_2)_6$. Alternative possibilities to B are possible with orthorhombic CuL_6 polyhedra.

The MO coefficient β of the d_{xy} orbital engaged in the in-plane π-bonding may be estimated by the approximate equation

$$u_z = \frac{\lambda}{E_z}\beta^2(\alpha^2 - \alpha\alpha'S) \tag{11}$$

One obtains from the orbital contribution $u_z = 0.034$ a β^2 value of about 0.93.

It may be interesting to compare our data with the results of INDO–LCAO–MO calculations on the $Cu(NO_2)_6^{4-}$ moiety.[17] While the α coefficient is comparable in magnitude to ours, the ratio R is 0.6, which would indicate only small ligand p contributions to the overlap with $d_{x^2-y^2}$. Also a considerable delocalization of the d-electron density toward the oxygen atoms is calculated, which we could not derive from the EPR data ($I = 0$ for ^{16}O). The calculated β coefficient is again very similar to the one obtained by us.

Exchange Interactions. The group of lines around $g = {}^1/_2(g_\parallel + g_\perp)$, separated by $\simeq$90 G, observed in the EPR spectra of semidiluted compounds (Figures 2B and 5) is due to exchange-coupled, antiferrodistortive dimers (Figure 7). The intensity of this pattern increases with the Cu^{2+} concentration and vanishes in the very dilute complexes. The signals do not disappear at 4.2 K. Even for the best signals of this type $[A_2Cd_{1.98}Cu_{0.02}(NO_2)_6$ (A = K, Rb)], the intensity ratios between the hyperfine components could not be determined exactly because of their low intensity. The fine structure may be analyzed in terms of the Hamiltonian given by Abragam and Bleaney ("dissimilar pairs"),[11] to which we added the contributions due to the hyperfine and electric dipole–dipole interactions:

$$\hat{H} = \beta\mathbf{H}(g_1S_{z1} + g_2S_{z2}) + A_1S_{z1}I_{z1} + A_2S_{z2}I_{z2} + JS_1S_2 + XS_{x1}S_{x2} + YS_{y1}S_{y2} + ZS_{z1}S_{z2} \tag{12}$$

The indexes 1 and 2 refer to the interacting species. J is the exchange integral and X, Y, and Z are the components of the dipole–dipole interaction tensor, which was calculated on the basis of a model according to Smith and Pilbrow.[26] For each combination of the nuclear m quantum numbers of the two copper nuclei four energy levels result:

$$W_{1(2)} = (J + Z)/4 \overset{+}{(-)} R/2 \qquad W_{3(4)} = -(J + Z)/4 \overset{+}{(-)} S/2$$
$$R = [(\beta Hg_1 + \beta Hg_2 + A_1m_1 + A_2m_2)^2 + (X - Y)^2/4]^{1/2}$$
$$S = [(\beta Hg_1 - \beta Hg_2 + A_1m_1 - A_2m_2)^2 + [(X + Y)/2 + J]^2]^{1/2} \tag{13}$$

where $g_1 = g_z$, $g_2 = g_x$ (g_y), $A_1 = A_z$, and $A_2 = A_x$ (A_y). For small ratios $Q = J/(g_1 - g_2)\beta_e H$, two doublets corresponding to the transitions $W_1 \rightarrow W_3$, W_4 and $W_2 \rightarrow W_3$, W_4 (neglecting the hyperfine structure and dipolar interactions) should be observed, in which the doublet components are approximately separated by J.[11,27] The hyperfine interactions split each line into four quartets, if $A_1 \neq A_2$. In case of large Q ratios only two transitions with measurable intensity ($W_1 \rightarrow W_3$ and $W_2 \rightarrow W_3$) are predicted, which may coincide at $g = (g_1 + g_2)/2$ (again without hyperfine

(24) Ammeter, J. H. Dissertation, ETH Zürich, 1969.
(25) Smith, D. W. *J. Chem. Soc. A* **1970**, 3108.
(26) Smith, T. D.; Pilbrow, J. R. *Coord. Chem. Rev.* **1974**, *13*, 173.
(27) van Kalkeren, G.; Keijzers, C. P.; Srinivasan, R.; De Boer, D.; Wood, J. S. *Mol. Phys.* **1983**, *48*, 1.

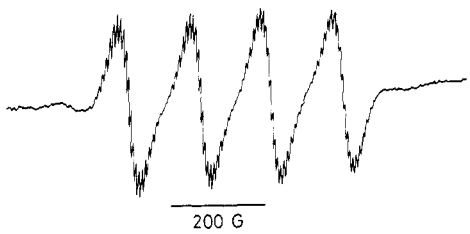

Figure 8. g_z part of the single-crystal EPR Q-band spectrum of $Tl_2Cd_{1.98}Cu_{0.02}(NO_2)_6$ parallel to a crystal axis (θ = 0°) at 77 K.

and dipolar interactions). The hyperfine splittings of the two transitions should converge toward four quartets with separations $A_z/2$ and $A_{x(y)}/2$, respectively. Our spectra are very near to the latter limit of large Q ratios. Though the simulation procedure with the pair geometries as shown in Figure 7B did not lead to a sufficiently good agreement with the experimental spectra (Figure 5C), we may estimate J to be about 0.6–0.7 cm^{-1}. This result is interesting with respect to $K_2PbCu(NO_2)_6$, for example, which is a linear antiferromagnet. From calorimetric measurements J = 2 cm^{-1} was found for the exchange interactions within the chain[28] (Figure 7A). The J integral, derived from our measurements, would correspond to the interchain interactions in this compound, which are considerably weaker and of the ferromagnetic coupling type. We did not try to improve the quality of the simulation by taking into account antiferrodistortive pair geometries in addition to those in Figure 7B, because the exchange part in our spectra was not sufficiently well resolved. Keijzers et al. investigated Cu^{2+}-doped $Zn(PNO)_6X_2$ complexes with respect to exchange interactions.[27] The derived J = 0.05 cm^{-1} is much smaller than our value and represents a situation with an intermediate Q ratio, where a pronounced dependence of the spectra also from the observation frequency was observed.

Tl SHF Structure. The EPR spectra of the diluted Tl complexes (Figure 8) differed significantly from the spectra of corresponding K, Rb, and Cs compounds. The superhyperfine structure in the $g_\parallel$ signal consisted of 23 lines separated by ≃6.5 G, quite different from the nine-line SHF structure due to four ^{14}N nuclei in the other compounds. Apparently the interaction of the unpaired electron of Cu^{2+} (atomic position 0, 0, 0) with the eight surrounding Tl nuclei in the $^1/_2$, $^1/_2$, $^1/_2$ positions of the pseudocubic unit cell causes this difference. We obtained good agreement between the experimental and simulated spectra, if we used the ^{14}N SHF constants A_x and A_y of Table III and A_{Tl} = 6.5 G. The nuclear spin quantum number of Tl is $^1/_2$, the nuclear magnetic moment[16] 1.611β_N, and the Cu–Tl spacing ≃4.5 Å. The dipolar part of the SHF interaction (cf. eq 2) is calculated to be A_d = 0.085 × 10^{-4} cm^{-1} = 0.08 G and hence by far too small to account for the observed splitting. The contact term is given by an expression analogous to eq 7: $A_{iso} = A^s_{Tl}\alpha''^2$, where α'' is the contribution of the Tl s orbitals to the ground-state wave function (eq 5). The A^s_{Tl} value of 6.1308 cm^{-1} is the largest of all elements[29] and leads to α'' = 1.06 × 10^{-2}. The significant contribution of Tl to the superhyperfine structure is obviously due to the very large nuclear magnetic moment and s-electron density at the Tl nuclei, though the delocalization of the unpaired Cu^{2+} electron at these atomic positions, which is measured by α'', is not significant at all.

The Additional Seven-Line SHF Structure. The additional signals on the weak-field side of the EPR spectra were one of the most interesting features of this study. They indicate Cu^{2+} polyhedra with only three nitrogen ligands in the xy plane (Figure 1). Information about the coordination on the z axis is not available, since the axial nitrogen atoms do not contribute to the SHF splitting. It is deduced from the angular dependence (Figure 4) that the g_z component of the unknown species lies in the xz plane, which is defined by the **g** tensor of the regular molecule. The x axis is most probably the one that involves the nitro group

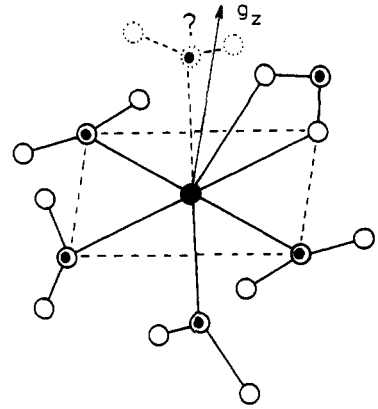

Figure 9. Cu^{2+} polyhedron with mixed nitro–nitrito coordination, which is thought to induce the additional low-field EPR spectrum of mixed crystals $A_2B_{2-x}Cu_x(NO_2)_6$. The g_z direction for this species (Figure 4) is also indicated.

oriented perpendicular to the xy plane (Figure 1). This should be so, because the Cu–N bonds along this direction are always the shortest (structural data)[30,31] and the g component correlated with the shortest bond is usually the smallest. We propose for the molecule giving the additional ESR spectrum a geometry according to Figure 9, with four nitro ligands and one nitrito group coordinated as a bidentate ligand via oxygen atoms. Cu^{2+} ions can indeed bind NO_2 groups via the oxygen atoms also.[4,32] This leads usually to a comparatively short Cu–O bond in the xy plane (≃2.2 Å). The out-of-plane Cu–O spacing is considerably longer (≃2.7 Å) and the respective O–Cu–O angle is about 50–55°. We feel that during the process of crystal growing the probability for a coordination of the bidentate nitrite ligand is highest on the x axis, because a nitro ligand in this position would have the same orientation (Figures 1 and 9). This geometry produces less strain than a coordination on the y axis. We cannot decide from our EPR data whether a sixth NO_2 group is present on the z axis or not. If it is present, the chelating nitro ligand can definitely not be located on the y axis because of obvious steric reasons. The g_z direction of the molecule in Figure 9 is indeed expected to be located in the xz plane, but it does not necessarily coincide with the molecular z axis. Four symmetry-equivalent orientations are possible, in which g_z is inclined by angles ±α and 180° ± α with respect to the z axis—in agreement with two different signals in the EPR experiment (α = 10°; Figure 4). The magnitude of g_z and A_z (larger and smaller than the values for the regular spectrum, respectively) are also consistent with a change from N to O ligator atoms. It is further interesting that the ^{14}N-SHF constants $A_x \simeq A_y$ are slightly smaller (12.7 × 10^{-4} cm^{-1}) than those of the regular $Cu(NO_2)_6$ entities (13.6 × 10^{-4} cm^{-1}). This observation indicates a weakening of the interaction between $d_{x^2-y^2}$ and the three nitro groups, which is possibly caused by a deviation from the planar geometry as the consequence of the presence of the chelating nitrito ligand.

We have presumed in the discussion above that the molecular axes of the regular polyhedra and the discussed species are parallel, because of the rigidity of the crystal structure. The concentration of the moieties with a nitro–nitrito coordination is only about 2% of the total copper concentration. In conclusion, we may state that EPR spectroscopy at higher frequencies is presumably the only physical method which can detect the species under discussion.

Conclusions

Electron paramagnetic resonance spectroscopy at higher microwave frequencies proved to be a very suitable probe technique for studying Cu^{2+} in a pseudooctahedral NO_2^- environment. The

(28) Huiskamp, W. J. *Ann. Acad. Sci. Fenn., Ser. A6* **1966**, No. 210.
(29) Morton, J. R.; Preston, K. F. J. *J. Magn. Reson.* **1978**, *30*, 577.
(30) Takagi, S.; Joesten, M. D.; Lehnert, P. G. *J. Am. Chem. Soc.* **1974**, *96*, 6606.
(31) Takagi, S.; Joesten, M. D.; Lehnert, P. G. *Acta Crystallogr., Sect. B: Struct. Crystallogr. Cryst. Chem.* **1975**, *B31*, 596; **1976**, *B32*, 2524.
(32) Klanderman, K. A.; Hamilton, W. C.; Bernal, I. *Inorg. Chim. Acta* **1977**, *23*, 117.

high resolution and sensitivity of this method allowed us to detect a very small percentage of Cu^{2+} polyhedra with a mixed nitro-nitrito coordination as well as the usual hexanitro species. Also the superhyperfine structure due to the interaction with the Tl nuclei was resolved in the spectra of the Tl complexes, due to a very weak spin delocalization toward the Tl^{+} cations. Signals originating from exchange-coupled Cu^{2+}-Cu^{2+} pairs were observed only at higher frequencies. Finally MO parameters for the Cu-N bonds could be derived from the experiments and compared with the results of theoretical calculations. The bonding and geometry of the Cu^{2+} polyhedra is strongly influenced by the Jahn-Teller effect.

Acknowledgment. One of the authors gratefully acknowledges the cooperation with Dr. G. F. Kokoszka (NATO grant) with respect to V-band EPR spectroscopy and line-shape effects.

Registry No. $K_2Cd_2(NO_2)_6$, 98542-08-6; $Rb_2Cd_2(NO_2)_6$, 85565-57-7; $Tl_2Cd_2(NO_2)_6$, 37956-94-8; $Cs_2Cd_2(NO_2)_6$, 37956-95-9; $Tl_2Hg_2(NO_2)_6$, 98542-09-7; $Cs_2Hg_2(NO_2)_6$, 37956-96-0; $Cs_2PdHg(NO_2)_6$, 98542-10-0; Cu^{2+}, 15158-11-9.

Contribution from the Department of Chemistry, The University of Chicago, Chicago, Illinois 60637

Energetic Description of Solids in Terms of Small Fragments

JEREMY K. BURDETT* and DUANE C. CANEVA

Received January 9, 1985

The following inorganic solids were studied, with use of both tight-binding band structure computations on the crystal and molecular orbital calculations on small fragments torn from the crystal lattice: α-BeO, cooperite, $PdCl_2$, β-tridymite, β-quartz, stishovite, and silica-w. Not only are the demands of the local angular geometry of both anion and cation important in determining the details of the structure but the energetics of the anionic matrix play an important role also. In all of these systems it appears that the repulsions between the closed shells of electrons associated with the anions are close to being minimized in the observed structure, subject to the constraint of constant anion-cation distance. Comments are made on the validity of geometrical and energetic data obtained from calculations on small molecular units torn from the lattice, which do not have the same stoichiometry as the solid.

Introduction

When we attempt to understand the factors that determine crystal structure with the aid of numerical calculations of one type or another, the problem that we invariably face is how to sort out from the numerology concepts and ideas that are useful in a qualitative as well as quantitative sense. In general, we feel particularly happy if we can attribute stability to geometrical features that involve small groups of atoms: in other words, focus on rather local effects. Bland statements of the type that structure A is more stable than structure B because it has a larger Madelung constant or lower total energy calculated via some quantum-mechanical method are less attractive in this regard.

A useful approach in the past decade or so has been the study of the energetics of relevant structural units[1-4] torn from the crystal lattice whose dangling bonds have been sealed with either electrons or hydrogen atoms. So, for example, studies of SiO_4^{4-}, $(SiH_3)_2O$, and analogous molecules where silicon has been replaced by aluminum or phosphorus have been invaluable in casting light on structural features of silicate materials.[2,3] In this paper we compare results obtained for a variety of systems using both molecular orbital calculations on small fragments and tight-binding calculations on crystalline structures. Exactly the same method and parameters are used in both areas (the extended Hückel ansatz), and so we hope not only to understand why these systems adopt the structures they do but also to investigate the validity of such local cluster calculations and see how good such one-electron methods are in reproducing the observed geometrical details of extended solid-state arrays. Although we shall use the terms anion and cation in this paper to represent respectively the more electropositive and electronegative atoms of the solid and will in fact only consider systems with a significant electronegativity difference between the constituents, we do not intend this usage to imply dominance of ionic interactions in bonding. In fact, we use an orbital picture of these solids where such Coulombic forces are not explicitly included.

α-Beryllia (BeO)

The lowest energy polymorph of BeO has the wurtzite structure. Elsewhere we have investigated[1a] the factors that locate this arrangement as the one of lowest energy, rather than another way of filling of the tetrahedral holes in the structure. The space group of the structure is $P6_3mc$ with the Be atoms in 2(a): (0, 0, u_1; $^1/_3$, $^2/_3$, $^1/_2 + u_1$) and the O atoms in 2(a) (0, 0, u_2; etc.) (Figure 1). There are therefore three degrees of freedom in this structure, the crystallographic parameters a, c and $u_1 - u_2$ (u). Fixing the axial (parallel to z) and basal Be-O distances (l) leads to one variable (u) so that

$$\gamma^2 = \frac{4}{12u - 3} \tag{1}$$

where $\gamma = c/a$, the axial ratio. The volume is given by

$$V = \frac{l^3(u - {}^1/_4)}{2u^3} \tag{2}$$

The maximum volume subject to this constraint occurs at $u = {}^3/_8$. Four sets of calculations were performed in which u was varied: (i) a band structure computation for the BeO crystal (see the Appendix for details.); (ii) a calculation, similar to (i) but where the Be atoms were missing and the lattice was considered as being made up of oxide anions; (iii) local geometry calculations for BeO_4^{6-} ions; (iv) local geometry calculations for OBe_4^{6+} ions. In the last two calculations interactions between the ligands were "switched off" so that the results measure the effect of geometry variation on local anion-cation interactions and the effect of the anion lattice is not double counted. At $u = {}^3/_8$ several geometrical features are in coincidence. First the oxide ions are in hexagonal eutaxy. (We use O'Keeffe's terminology[5,6] here to describe the arrangement of ions whose centers are located at the centers of hard spheres in a closest packing. In this way we remove from discussion the nebulous concept of "ionic size".) Second, both oxygen and beryllium geometries are exactly tetrahedral. For real molecules with such electronic configurations this of course is the geometry expected. Figure 2 shows the energetics associated with the set of calculations described above, and also an estimate of the total energy variation with u as a weighted sum of the indi-

(1) (a) Burdett, J. K.; McLarnan, T. J. *Am. Mineral.* **1984**, *69*, 601. (b) Burdett, J. K.; McLarnan, T. J. *J. Chem. Phys.* **1981**, *75*, 7554.
(2) (a) O'Keeffe, M., Navrotsky, A., Ed. "The Structures of Complex Solids"; Academic Press: New York, 1981. (b) Gibbs, G. V. In ref 2a.
(3) (a) Lager, G. A.; Gibbs, G. V. *Am. Mineral.* **1973**, *58*, 756. (b) O'Keeffe, M.; Gibbs, G. V. *J. Chem. Phys.* **1984**, *81*, 876. (c) Gibbs, G. V. *Am. Mineral.* **1982**, *67*, 421.
(4) Tossell, J. A. *Trans. Am. Crystallogr. Assoc.* **1979**, *15*, 47.
(5) O'Keeffe, M. *Acta Crystallogr., Sect. A: Cryst. Phys., Diffr., Theor. Gen. Crystallogr.* **1977**, *A33*, 924.
(6) O'Keeffe, M. In ref 2a.

0020-1669/85/1324-3866$01.50/0